Acoustic Weyl points in a square lattice

Ting-Gui Chen, Jun-Rui Jiao, Hong-Qing Dai, and De-Jie Yu*
State Key Laboratory of Advanced Design and Manufacturing for Vehicle Body, College of Mechanical and Vehicle Engineering, Hunan University, Changsha, Hunan 410082, China

(Received 4 September 2018; published 18 December 2018; corrected 21 December 2018)

We show that acoustic double Weyl points are observed in a square lattice by breaking inversion symmetry. We also show that the double Weyl points are protected by the C_4 rotation symmetry but are unaffected by translation symmetry along the z direction. When C_4 rotation symmetry is broken, the double Weyl point will split into two single Weyl points in the x-y plane. Gapless surface states and backscattering immune properties are demonstrated in double and single Weyl systems. The topologically protected one-way propagation of sound waves is demonstrated experimentally. The acoustic Weyl points obtained in the easily fabricated square lattice structure will provide a platform to study the topological properties and lead to potential applications in acoustic devices.

DOI: 10.1103/PhysRevB.98.214110

I. INTRODUCTION

Recently, Weyl semimetals of classical wave systems have attracted a lot of attention [1–21]. A Weyl point can be viewed as a topological singular point which is a source or sink of the Berry curvature flux in momentum space [22]. Crucially, such a Weyl point is characterized by an integer-valued topological charge. This topological charge describes the singularity in the eigenstates near the crossing point corresponding to the chirality of the Weyl fermion [2,7]. A Weyl point, which is a doubly degenerate point with linear dispersions along all directions, can also be viewed as a three-dimensional (3D) extension of a two-dimensional (2D) Dirac point [2]. However, differing from the unstable Dirac points, Weyl points are topologically stable against perturbation and virtually indestructible, unless two Weyl points of opposite topological charges annihilate each other [7]. Their robustness to perturbations is attributed to the exhausted degrees of freedom in the Weyl Hamiltonian, so that perturbations respecting the translational symmetry cannot lift the degeneracy but can only shift the position of the Weyl points [2]. Nevertheless, the existence of topologically protected Weyl points does not require a particular symmetry. It is just known that the existence of Weyl points requires the absence of time-reversal symmetry or space-inversion symmetry (or both of them). Because inversion symmetry requires a Weyl point located at point k on the Brillouin zone (BZ) to have a partner of opposite charge at $-k$. Time-reversal symmetry requires a Weyl point located at k to have a partner of the same charge at $-k$, which implies that for a system with both time-reversal and space-inversion symmetries, the topological charge must be zero [2,6]. All these limitations make acoustic systems that exhibit Weyl points more challenging.

Differing from the electronic or optical systems, it is difficult to break time-reversal symmetry in acoustic systems [22]. Therefore, in order to realize acoustic Weyl semimetals, it is necessary to design a geometric structure without space-inversion symmetry [6]. In the last few years, Weyl points have been found in classical wave systems such as photonic and acoustic systems [2,5,7,9,11,16,18–22]. The Weyl points beyond nature have been firstly reported in photonic crystals based on double-gyroid structures [16] and the topologically nontrivial surface states have been demonstrated experimentally [13,16]. However, for classical waves, the gyroid structure is very complicated to fabricate. Besides the gyroid structures' crystals, Weyl points can also be fabricated using planar fabrication technology based on a layer-stacking strategy [2,7,8]. More recently, photonic crystals with multiple Weyl points have been fabricated and the robustness of these surface states against k_z-preserving scatting has been experimentally observed [2]. Inspired by the developments of photonic crystals, some achievements of Weyl points have been made in phononic crystals. Weyl points are closely related to the synthetic gauge flux in the three-dimensional band structures [5]. The surface states have been demonstrated in a chiral phononic crystal system with Weyl points [22]. Very recently, Weyl points have been observed in these very easily fabricated woodpile crystals [7,20,21]. These woodpile crystals with multiple Weyl points have been firstly observed in optical systems [7]. Soon after, negative refraction of topological surface waves [20] and topologically protected one-way propagation of acoustic waves [21] have been demonstrated experimentally in phononic crystals, respectively. These easily fabricated woodpile crystals suggest that it may be possible to obtain Weyl points in a square lattice.

To date, the researchers have made a great effort to obtain Weyl points in acoustic systems, but most of the phononic crystals with Weyl points are proposed in grapheme-based structures in a honeycomb lattice [5,19–22]. Although the honeycomb lattice has been proved to be a very successful platform for designing acoustic Weyl semimetal materials, the nonhoneycomb systems with Weyl points [9] need to be explored further. Generally, phononic crystals with complicated gyroid structures or single grapheme-based structures in a

*djyu@hnu.edu.cn

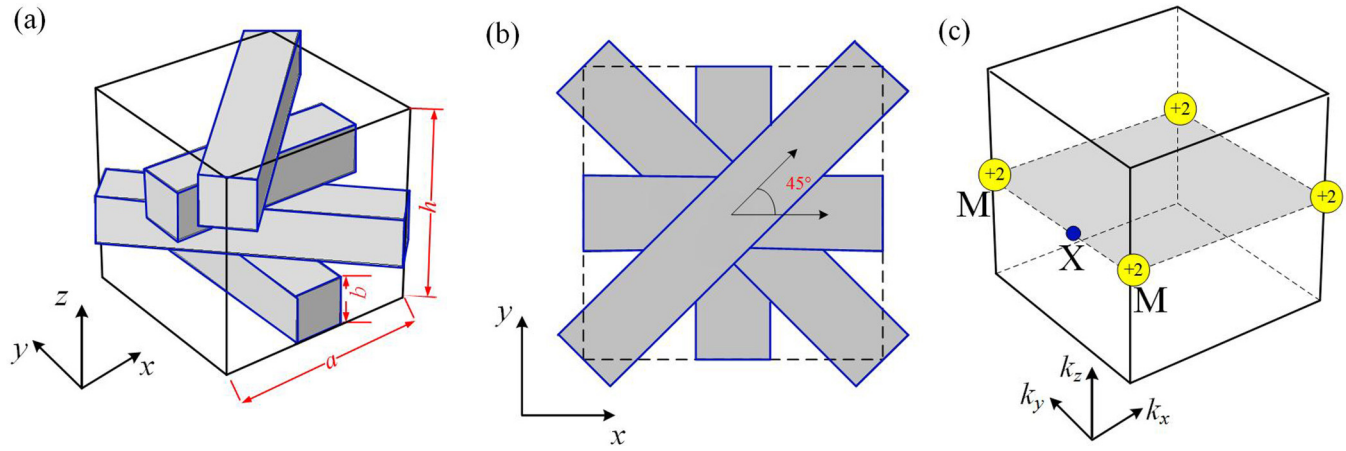

FIG. 1. Illustrations of the unit cell of the acoustic system. (a) The unit cell contains four layers of rotated rods. (b) Top view of unit cell (dashed square). (c) The first BZ of the acoustic system. The system at $k_z = 0$ has a 2D band structure in the reduced BZ [light gray plane in (c)]. The yellow spheres represent the double Weyl points with topological charges +2, and the M and X nodes are high-symmetry points.

honeycomb lattice are not convenient for the study of acoustic Weyl semimetals. Therefore, it is necessary to design easily fabricated square lattice structures carrying Weyl points in acoustic systems to study the topological properties. Notably, the double Weyl points, whose dispersion is quadratic along the k_x and k_y directions and linear along the k_z direction with topological charges of ± 2, are protected by C_4 or C_6 symmetries [23–25]. Double Weyl points with time-reversal and C_3 rotational symmetry have been very recently experimentally implemented in photonic crystals [2]. When the symmetries are broken, the double Weyl point will split into two single Weyl points [2,24,26,27]. This fact suggests that it may be possible to obtain Weyl points by splitting double Weyl points.

In this paper, we design an acoustic Weyl semimetal in a square lattice by breaking inversion symmetry. The acoustic Weyl semimetal is combined with stacked rods which can be easily fabricated. Firstly, we observe an acoustic double Weyl point in a square lattice. Secondly, we discuss the effects of the reduced symmetries on double Weyl points. Finally, we experimentally demonstrate the topologically protected one-way propagation of sound waves in acoustic Weyl semimetal materials.

II. SYMMETRY ANALYSIS OF WEYL POINTS

Near the Weyl points, the band structures are described by the Hamiltonian

$$H(k) = \sum_{ij} \Delta k_i v_{ij} \sigma_j \quad (i, j = x,\ y \text{ or } z), \tag{1}$$

where $\Delta k_i = k_i - k_0$ is the wave vector relative to the position k_0 of the Weyl point, v_{ij} is an invertible effective velocity matrix describing the band crossing at the first order in Δk_i, and σ_j indicates the Pauli matrices. Especially, Weyl points and the associated topological charge enable the Weyl semimetals to exhibit a variety of unusual properties, such as robust surface states and one-way propagation [2,8,21,22].

Weyl points are more stable than Dirac points but are more elusive entities. It is difficult to obtain Weyl points in a particular symmetry directly. Notably, the existence of Weyl points requires the absence of time-reversal symmetry or space-inversion symmetry. Hence, we design a chiral acoustic system without inversion symmetry. The unit cell consists of four layers of rods with width b and height b. Each layer is rotated 45° anticlockwise from the layer below as shown in Fig. 1(a). The total height of the unit cell is $h = 4 \times b$. All the four layers are twisted up along the z direction while forming a square lattice in the x-y plane. The top view of the unit cell (dashed square with length a) is shown in Fig. 1(b). The first BZ of the unit cell is shown in Fig. 1(c). For any 3D system, k_z can be viewed as a parameter characterizing the topological characteristics in a 2D system, so the light gray plane can be seen as a 2D BZ at $k_z = 0$. The yellow spheres represent the distribution of double Weyl points with topological charges +2, and the M and X nodes are high-symmetry points that we care about in this paper.

Obviously, this acoustic system is invariant under a four-fold rotation operator and a simultaneous partial translation of the $h/2$ operator along the z direction, as the system is preserved by screw symmetry expressed as $C_{4,2} = C_4 T_{h/2}$. Hence, after applying the screw symmetry operator four times, we can obtain $C_{4,2}^4 = (T_{h/2})^4 = T_{2h}$. Due to the periodicity, the Bloch wave function satisfies $\phi(\vec{r}) = u(\vec{r})e^{-i\vec{k}\vec{r}}$; thus

$$C_{4,2}^4 \phi(\vec{r}) = T_{2h}\phi(\vec{r}) = \phi(\vec{r})e^{-i2k_z h}. \tag{2}$$

Therefore, the eigenvalue of the operator of $C_{4,2}^4$ is in the form $J_m = e^{im\pi/2}e^{-ik_z h/2}$, where $m = 0, 1, 2, 3$. Due to the periodicity, at the k_z zone boundaries where $k_z = \pm\pi$, we can obtain

$$\begin{aligned} J_0(k_z h/2) &= J_2(k_z h/2 + \pi), \\ J_2(k_z h/2) &= J_0(k_z h/2 + \pi), \end{aligned} \tag{3}$$

$$\begin{aligned} J_1(k_z h/2) &= J_3(k_z h/2 + \pi), \\ J_3(k_z h/2) &= J_1(k_z h/2 + \pi). \end{aligned} \tag{4}$$

The eigenvalues J_0 and J_2 (or J_1 and J_3) for different representations of screw symmetry should connect at the zone boundaries in the extended BZ. For a general dispersion of

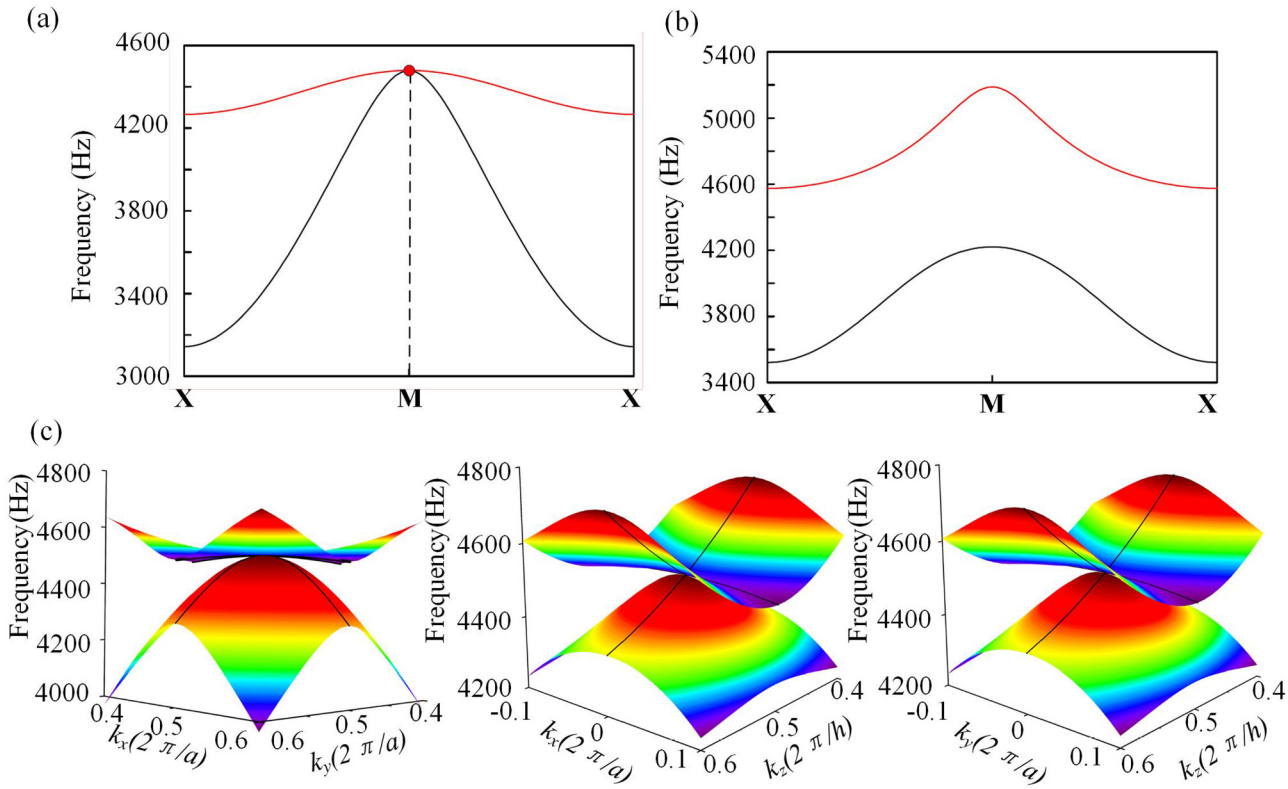

FIG. 2. The band structures of the lowest two bands. The band structures of the unit cell along the *XM* direction in the k_x-k_y plane at $k_z = 0$ (a) and $k_z = 0.5\pi/h$ (b). A doubly degenerate point is found at the *M* node. (c) Three-dimensional band structures of the unit cell around the *M* node in the k_x-k_y plane (left), the k_x-k_z plane (middle), and the k_y-k_z plane (right), respectively.

three bands along the *XM* direction in the extended zone scheme, the bands can fold back to the first BZ to form two unavoidable crossing points. However, when the time-reversal symmetry is preserved, the Hamiltonian satisfies

$$T H(0, 0, k_z) T^{-1} = H(0, 0, -k_z), \tag{5}$$

and due to the screw symmetry and bands folding, the Hamiltonian also satisfies

$$C_{4,2} H(k) C_{4,2}^{-1} = H(R_4 k), \tag{6}$$

where $C_{4,2}$ is the fourfold rotation and translation operator and R_4 is the rotation matrix defining the 3D fourfold rotation. The constraints on Eqs. (5) and (6) require that the bands should be symmetric about $k_z = 0$ along the z direction. After band folding to the first BZ, the crossing points should locate at $k_z = 0$ or k_z boundaries.

In order to obtain the topological charge of a double Weyl point, we calculated the topological charge by analyzing the rotational eigenvalues of the two touching bands [23]. If we choose the eigenfunctions of $C_{4,2}$ as the basis, at the *M* node, the matrix representation of $C_{4,2}$ is given by

$$C_{4,2} = e^{i[(m_1+m_2)/2]\pi} e^{i[(m_1-m_2)/2]\pi\sigma_z} e^{-ik_z p/2}, \tag{7}$$

where m_1 and m_2 are the eigenvalues of $C_{4,2}$; they are also the eigenvalues of the first and the second bands. Near this two-band crossing point (*M* node), we can obtain the effective Hamiltonian as

$$H_{\text{eff}}(k) = f(\Delta k)\sigma_+ + f^*(\Delta k)\sigma_- + g(\Delta k)\sigma_z. \tag{8}$$

In the above equation, Δk is the wave vector deviation of the *M* node, f is a complex function, g is a real function, and $\sigma_\pm = \sigma_x \pm i\sigma_y$. The transform of $H_{\text{eff}}(k)$ under $C_{4,2}$ is given by

$$\begin{aligned} C_{4,2} H_{\text{eff}}(k) C_{4,2}^{-1} = {} & f(\Delta k) e^{i[(m_1-m_2)/2]\pi}\sigma_+ \\ & + f^*(\Delta k) e^{-i[(m_1-m_2)/2]\pi}\sigma_- + g(\Delta k)\sigma_z \end{aligned} \tag{9}$$

Meanwhile, $R_4 k$ is given by

$$R_4(k_+, k_-) = (k_+ e^{i\pi/2}, k_- e^{i\pi/2}), \tag{10}$$

where $k_\pm = k_x \pm i k_y$. By substituting Eqs. (9) and (10) into Eq. (7), we obtain

$$\begin{aligned} & e^{-i[(m_1-m_2)/2]\pi} f(\Delta k_+, \Delta k_-) \\ & = f(\Delta k_+ e^{i\pi/2}, \Delta k_- e^{i\pi/2}) g(\Delta k_+, \Delta k_-) \\ & = g(\Delta k_+ e^{i\pi/2}, \Delta k_- e^{i\pi/2}). \end{aligned} \tag{11}$$

This is the general constraint on f and g by $C_{4,2}$ symmetry. We can expand the $f(\Delta k_+, \Delta k_-)$ near the *M* node as follows:

$$f(\Delta k_+, \Delta k_-) = \sum_{n_1 n_2} A_{n_1 n_2} \Delta k_+^{n_1} \Delta k_-^{n_2}, \tag{12}$$

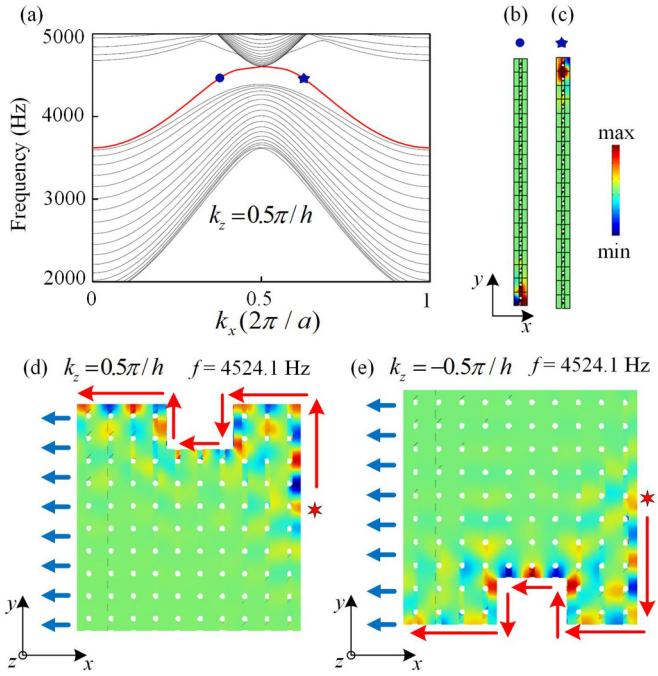

FIG. 3. The bulk band structures and surface states. (a) The bulk band structures of the supercell in the k_x-k_y plane at $k_z = 0.5\pi/h$ along the k_x direction. Surface band (red band) exists in the nontrivial gap. (b,c) Eigenpressure fields of surface modes at $k_x = 0.8\pi/a$ (marked by blue dot) and $k_x = 1.2\pi/a$ (marked by blue star). (d,e) One-way propagation along the U-type boundary at the same frequency in different directions with different signs of k_z. The red star is the sound source. The direction of propagation is illustrated by the red arrows. The blue arrows indicate that the sound waves could leak out at the air boundary.

where $A_{n_1 n_2}$ is an arbitrary complex coefficient. Equation (11) requires that

$$A_{n_1 n_2} = 0 \quad \text{if} \quad n_2 - n_1 \neq m_1 - m_2 \mod 4. \tag{13}$$

Then we take the smallest $n_1 + n_2$ and nonzero $A_{n_1 n_2}$ to obtain the last column of Table I in Ref. [23]. The results indicate the crossing point at the M node should carry topological charges of $+2$.

III. REALIZATION OF WEYL POINTS

To show that acoustic Weyl points can exist in a square lattice, we design a unit cell whose parameters are, respectively, $a = 40$ mm, $b = 10$ mm, and $h = 40$ mm. The 3D band structures of the unit cell are calculated as shown in Figs. 2(a) and 2(b). According to the symmetry analysis of Weyl points, the band crossing points must be at the $k_z = 0$ or at the k_z zone boundaries when the time-reversal symmetry is preserved. In this acoustic system, when we set $k_z = 0$, the lowest two bands form a degenerate point in 3D momentum space at the M node as shown in Fig. 2(a). When k_z is increased, the degenerate point opens up and then a band gap appears. The gap reaches maximum as shown in Fig. 2(b) when k_z is around $0.5\pi/h$. To verify that the doubly degenerate point is a double Weyl point, we further calculate the topological charge and the 3D band structures in Fig. 2(c). It clearly shows that bands around the M node are quadratic along the k_x and k_y directions but linear along the k_z direction. The topological charges are $+2$, so the degenerate point is definitely a double Weyl point which can be seen as the superposition of two single Weyl points.

In the electronic or optical systems, the nonzero values of the gap Chern number induce topologically protected surface states [18,28]. To investigate the gapless surface states of double Weyl points, we construct a supercell consisting of a row of unit cells along the y direction that is periodic along the x and z directions. The hard boundaries are applied at two ends of this supercell as a topologically trivial system, and then we can obtain the corresponding bulk band structures as shown in Fig. 3(a). For $k_z = 0.5\pi/h$, we find that the gapless surface band (red band) exists in a topologically nontrivial gap. Obviously, the bulk band structures are symmetrical on $k_x = \pi/a$. We take the two gapless surface modes in the topologically nontrivial gap at $k_x = 0.8\pi/a$ (marked by blue dot) and $k_x = 1.2\pi/a$ (marked by blue star) respectively. The two surface modes are located at the bottom and top boundaries,

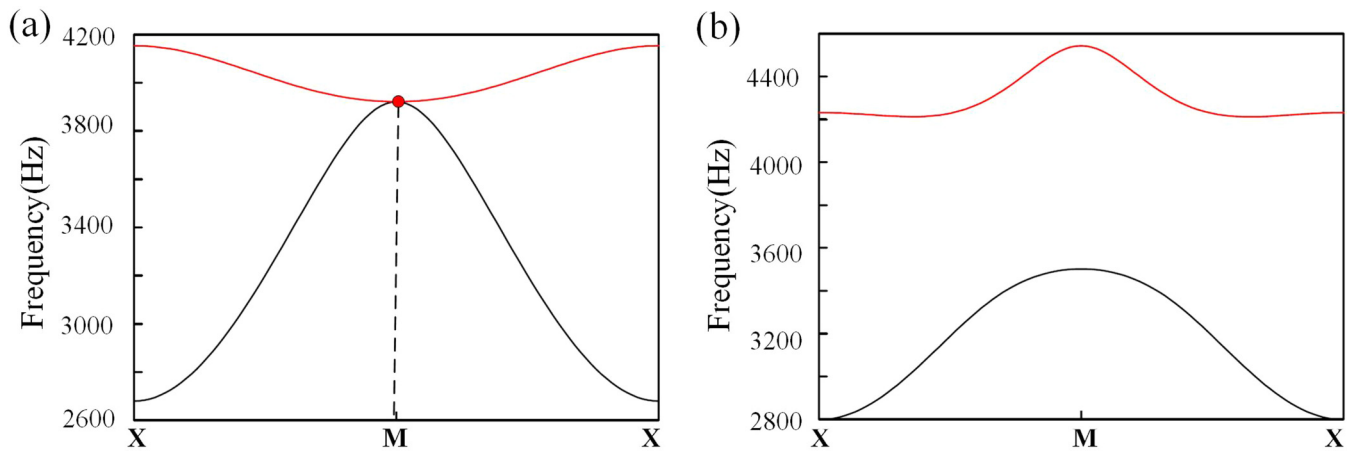

FIG. 4. The band structures of the lowest two bands after the height of the unit cell changed. The band structures of the unit cell along the XM direction in the k_x-k_y plane at $k_z = 0$ (a) and $k_z = 0.5\pi/h$ (b).

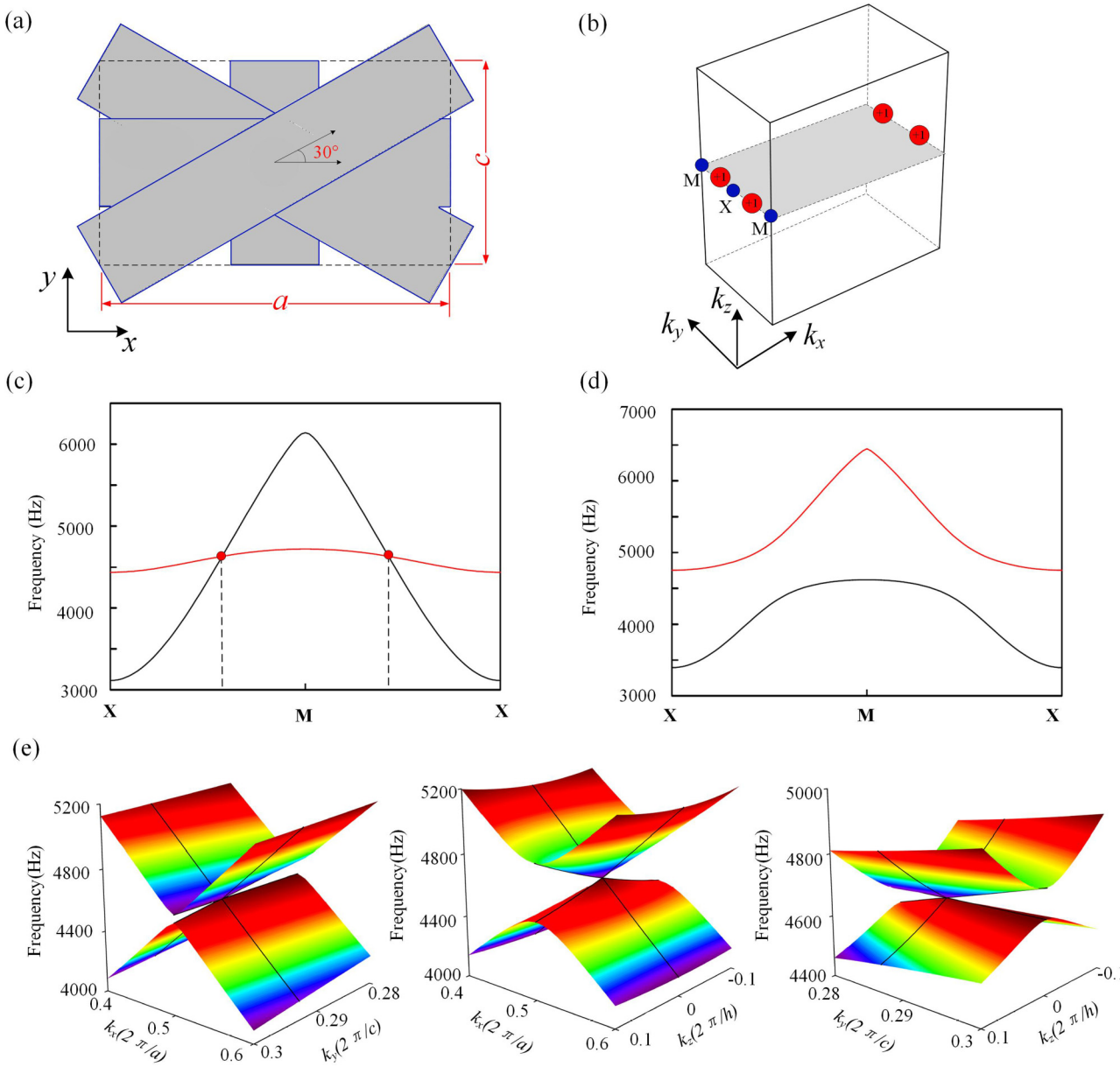

FIG. 5. The double Weyl point splits into two single Weyl points due to C_4 symmetry breaking. (a) Top view of the unit cell (dashed rectangle) of the acoustic system. (b) The first BZ of the acoustic system. The system at $k_z = 0$ has a 2D band structure in the reduced BZ ([ight gray plane in (b)]. The red spheres represent the single Weyl points with topological charge $+1$, and the M and X nodes are high-symmetry points. (c,d) the band structures of the unit cell along the XM direction in the k_x-k_y plane at $k_z = 0$ and $k_z = 0.5\pi/h$, respectively. The double Weyl point split into two single Weyl points illustrated by red dots in (c). (e) Three-dimensional band structures of the unit cell around the left red dot at $k_y = 0.574\pi/c$ in the k_x-k_y plane (left), the k_x-k_z plane (middle), and the k_y-k_z plane (right).

respectively, as shown in Figs. 3(b) and 3(c). Especially, the surface states located at the bottom and top boundaries propagate along the $+x$ and $-x$ directions, respectively. Therefore, the propagation of sound waves is efficiently prevented by the bulk gap, and the surface states will induce a topologically protected one-way propagation.

In order to investigate the robustness of surface states against backscattering when k_z is preserved, we construct a square acoustic system consisting of 10×10 unit cells whose top, right, and bottom boundaries are rigid. The left boundary is set as a scattering boundary so that the sound waves can perfectly leak out. The periodic condition is applied along the z direction in this acoustic system. To demonstrate the robustness of the surface states, we remove several unit cells from the top boundary to form the U-type boundary as shown in Fig. 3(d). Then we place a sound source (red star) in the middle of the right boundary and set $k_z = 0.5\pi/h$. Meanwhile, we set $f = 4524.1$ Hz, which is the excited frequency of the nontrivial gap. The sound waves robustly propagate in an anticlockwise direction along the boundary of the acoustic system, immunizing against corners and the U-type boundary without backscattering. When we remove several unit cells from the bottom boundary to form the U-type boundary and set $k_z = -0.5\pi/h$ at the same frequency, $f = 4524.1$ Hz, the

sound waves robustly propagate in a clockwise direction along the boundary of the acoustic system without backscattering as shown in Fig. 3(e).

IV. EFFECTS OF SYMMETRY ON DOUBLE WEYL POINTS

Note that double Weyl points are protected by the screw symmetry and they are not topologically stable [23–25]. If the symmetry is reduced, the double Weyl point will split into two single Weyl points and move away from the high-symmetry line. In this section, we explore the effects of reducing the point symmetry on double Weyl points. The screw rotation operations can be viewed as composite operations of translation and rotation, namely, $C_{4,2} = C_4 T_{h/2}$. Firstly, we change the translation symmetry by changing the height of the unit cell. The height of the unit cell is closely related to the height of the stacked rods. We only change the height of the rods from $b = 10\,\text{mm}$ to $b = 14\,\text{mm}$ along the z direction. The corresponding band structures at $k_z = 0$ and $k_z = 0.5\pi/h$ are plotted in Figs. 4(a) and 4(b), respectively. Compared with Fig. 2(a), the doubly degenerate point still exists at $k_z = 0$, so the change of the translation symmetry has no effect on double Weyl points. Secondly, we reduce the rotation symmetry by changing the length or width of the unit cell in the x-y plane. We construct a new unit cell with stacked rods whose height and width are $b = 10\,\text{mm}$. The first and third layers are rotated 60° anticlockwise but the second and the fourth layers are rotated 30° anticlockwise from the layer below. The top view of the new unit cell (dashed rectangle with length a and width c) is shown in Fig. 5(a), where $a = 40\,\text{mm}$ and $c = 23.10\,\text{mm}$. The first BZ of the new unit cell is shown in Fig. 5(b). The light gray plane can be seen as a 2D BZ at $k_z = 0$. The red spheres represent the distribution of single Weyl points with topological charge $+1$, and the M and X nodes are high-symmetry points. The band structures are plotted in Figs. 5(c) and 5(d) at $k_z = 0$ and $k_z = 0.5\pi/h$, respectively. Compared with the Fig. 2(a), the double Weyl point splits into two degenerate points, respectively, at $k_z = 0$ as shown in Fig. 5(c). To verify that the degenerate point is a single Weyl point at $k_y = 0.574\pi/c$ (or $k_y = 1.426\pi/c$), we further calculate the 3D band structures as shown in Fig. 5(e). It can be clearly seen from Fig. 5(e) that bands around the M node are linear along all directions. The topological charge is $+1$, so the degenerate point is definitely a single Weyl point.

To investigate the gapless surface states and transmission property of single Weyl points, we also construct a supercell, which consists of a row of unit cells along the y direction and is periodic along the x and z directions. The hard boundaries

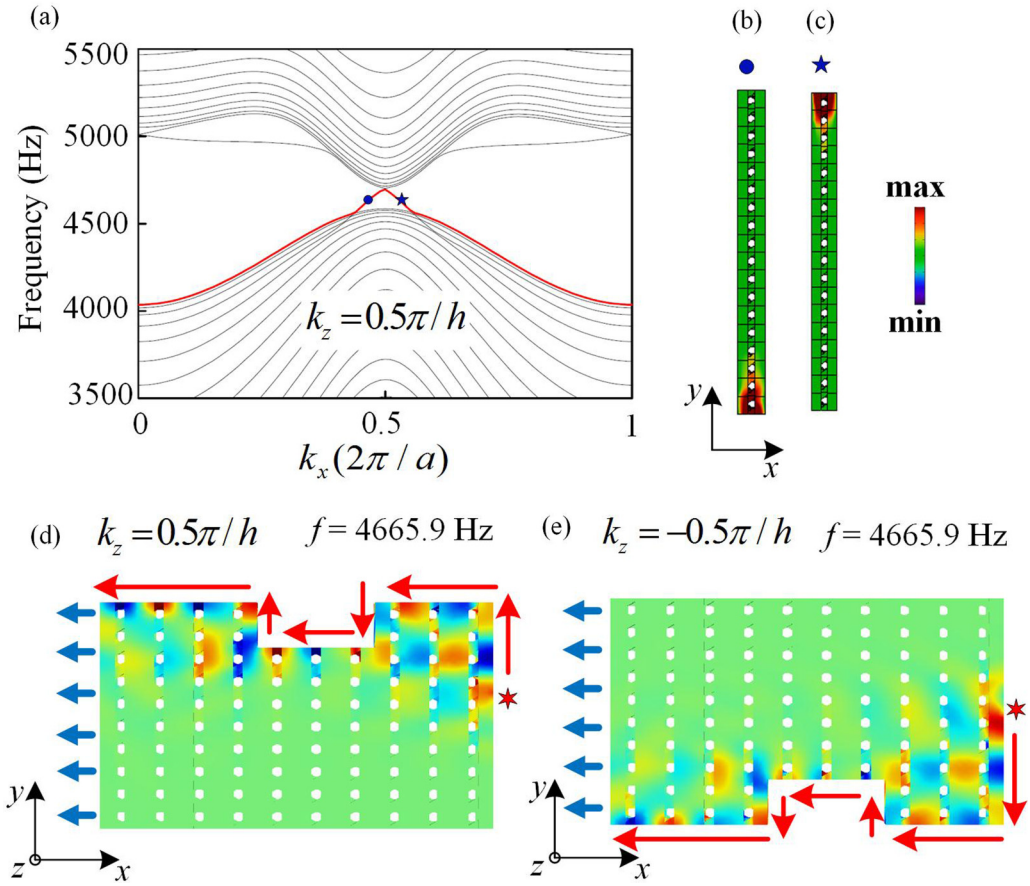

FIG. 6. The bulk band structures and surface states. (a) The bulk band structures of the supercell in the k_x-k_y plane at $k_z = 0.5\pi/h$ along the k_x direction. Surface band (red band) exists in the nontrivial gap. (b,c) Eigenpressure fields of surface modes found at $k_x = 0.94\pi/a$ (marked by blue dot) and $k_x = 1.06\pi/a$ (marked by blue star). (d,e) One-way propagation along the U-type boundary in different directions with different signs of k_z. The red star is the sound source. The direction of propagation is illustrated by the red arrows. The blue arrows indicate that the sound waves can leak out at the air boundary.

are applied at two ends of this supercell as a topologically trivial system; thus we can obtain the corresponding bulk band structures. For $k_z = 0.5\pi/h$, we find that the gapless surface band (red band) exists in the topologically nontrivial gap as shown in Fig. 6(a). Obviously, the bulk band structures are symmetric on $k_x = \pi/a$. We take the two gapless surface modes in the topologically nontrivial gap marked by the blue dot and star at $k_x = 0.94\pi/a$ (marked by the blue dot) and $k_x = 1.06\pi/a$ (marked by the blue star), respectively. The two surface modes are located at the bottom and top boundaries as shown in Figs. 6(b) and 6(c), respectively. As we know, the surface states located at the bottom and top boundaries propagate along the $+x$ and $-x$ directions, respectively. Therefore, the propagation of sound waves is efficiently prevented by the bulk gap, and the surface states will induce a topologically protected one-way propagation.

In order to investigate the robustness of surface states against backscattering when k_z is preserved, we construct a rectangular acoustic system consisting of 10×10 unit cells whose top, right, and bottom boundaries are rigid as shown in Fig. 6(d). The left boundary is set as a scattering boundary so that the sound waves can perfectly leak out. The periodic condition is applied along the z direction in this acoustic system. In order to demonstrate the robustness of the surface states, we remove several unit cells from the top boundary to form the U-type boundary. We place a sound source (red star) in the middle of the right boundary and set $k_z = 0.5\pi/h$. Meanwhile, we set $f = 4665.9$ Hz, which is the excited frequency of the nontrivial gap. The sound waves robustly propagate in an anticlockwise direction along the boundary of the acoustic system, immunizing against corners and the U-type boundary without backscattering. On the contrary,when we remove several unit cells from the bottom boundary to form the U-type boundary and set $k_z = -0.5\pi/h$ at the same frequency, $f = 4665.9$ Hz, the sound waves robustly propagate in a clockwise direction along the boundary of the acoustic system without backscattering as shown in Fig. 6(e). However, the nontrivial gap in the changed unit cell is relatively small, the surface states are more difficult to excite due to the disturbance of other bands.

V. EXPERIMENTS

In order to demonstate the topologically protected one-way propagation of sound waves in experiment, we construct a cubic acoustic system with stacked and rotated rodconsisting of $10 \times 10 \times 10$ unit cells as shown in Fig. 7(a). To excite the surface states with $k_z = 0.5\pi/h$, we place two sequential point sources in the first and second layer marked by a red and a yellow star. The two point sources are with identical frequencies, $f = 4552.5$ Hz, but phases increasing by $\pi/2$ from the first layer (marked by a red star). The loudspeakers connected with narrow tubes can be regard as the pointlike sources in the experiment. All the boundaries of this cubic acoustic system are set as hard boundaries, except the top boundary is set as a scattering boundary. The measured field distributions of acoustic pressure, as shown in Fig. 7(c), are scanned point by point through a microphone inserted into the sample. The experimental results in Fig. 7(c) are roughly consistent with the theoretical prediction in Fig. 7(b). The white

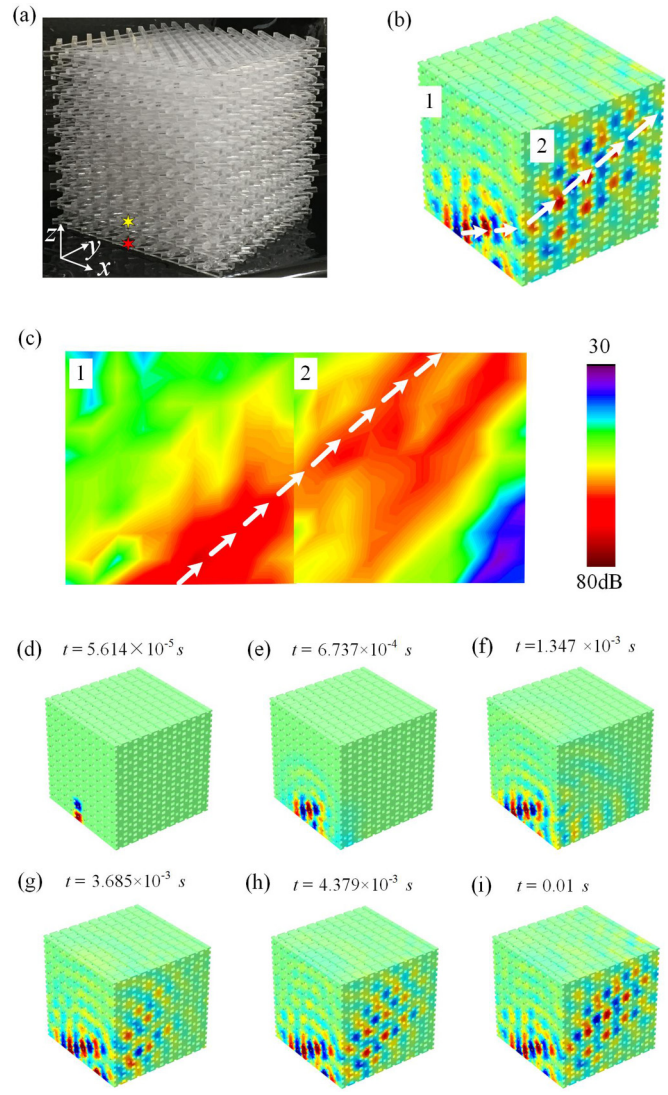

FIG. 7. Topologically protected one-way propagation of sound waves in the experiment. (a) The diagram of the acoustic system. The red and yellow stars represent the position of sound sources but with different phases in the experiment. (b) Theoretical predicted field distribution of acoustic pressure at $k_z = 0.5\pi/h$ and $f = 4552.5$ Hz. (c) Measured field distribution of acoustic pressure. The labels 1 and 2 represent planes 1 and 2 in (b). (d–i) Transient field distributions of acoustic pressure at different times. The sound wave propagates along the boundary of the cubic acoustic system in an anticlockwise direction.

arrows in both figures indicate the direction of sound wave propagation. The larger propagation angle is caused by the pointlike sources being placed not parallel but at a certain angle in the experiment. The another propagation route of sound waves in plane 2 is caused by the scattering of the bottom which cannot be neglected even in the theoretical prediction. Considering the decay of energy during the propagation due to the absorption in air, we only show the propagation of sound waves in planes 1 and 2 ([abeled in Figs. 7(b) and 7(c)]. The transient field distributions of sound wave propragation at different times in this acoustic system are displayed in Figs. 7(d)–7(i). To demonstrate such topologically protected

one-way propagation clearer, the field distributions of acoustic presssure in this set of figures [Figs. 7(d)–7(i)] are measured in unequal time intervals. The measured results in this set of figures show that the sound waves can propagate only in an anticlockwise manner along the boundary without obvious reflection or backscattering.

VI. CONCLUSION

We have designed an acoustic Weyl semimetal with double Weyl points by breaking inversion symmetry. Meanwhile, we have explored the effect of reducing symmetry on double Weyl points. We find that the translation symmetry along the z direction has no effect on double Weyl points but C_4 rotation symmetry does. The double Weyl point cannot split into two single Weyl points unless we break the C_4 rotation symmetry. The effect of symmetry on double Weyl points indicates that Weyl points can be obtained by breaking rotation symmetry of a double Weyl point. Furthermore, we demonstrate gapless surface states and backscattering immune properties in double and single Weyl systems. We also experimentally demonstrate topologically protected one-way propagation of sound waves in the cubic acoustic system. Moreover, obtaining Weyl points in an acoustic system with easily fabricated square lattice structures will provide a platform to study the topological properties and lead to potential applications in acoustic devices.

ACKNOWLEDGMENT

This study was supported by the National Natural Science Foundation of China (Grants No. 11572121 and No. 11402083).

[1] W. Gao, B. Yang, M. Lawrence, F. Fang, B. Beri, and S. Zhang, Nat. Commun. **7**, 12435 (2016).
[2] W. J. Chen, M. Xiao, and C. T. Chan, Nat. Commun. **7**, 13038 (2016).
[3] M. Xiao, Q. Lin, and S. Fan, Phys. Rev. Lett. **117**, 057401 (2016).
[4] D. Z. Rocklin, B. G. Chen, M. Falk, V. Vitelli, and T. C. Lubensky, Phys. Rev. Lett. **116**, 135503 (2016).
[5] M. Xiao, W.-J. Chen, W.-Y. He, and C. T. Chan, Nat. Phys. **11**, 920 (2015).
[6] M. Fruchart, S. Y. Jeon, K. Hur, V. Cheianov, U. Wiesner, and V. Vitelli, Proc. Natl. Acad. Sci. U. S. A. **115**, E3655 (2018).
[7] M.-L. Chang, M. Xiao, W.-J. Chen, and C. T. Chan, Phys. Rev. B **95**, 125136 (2017).
[8] R. Bi and Z. Wang, Phys. Rev. B **92**, 241109 (2015).
[9] Z. Yang and B. Zhang, Phys. Rev. Lett. **117**, 224301 (2016).
[10] D. Liu and J. Shi, Phys. Rev. Lett. **119**, 075301 (2017).
[11] S. H. Mousavi, A. B. Khanikaev, and Z. Wang, Nat. Commun. **6**, 8682 (2015).
[12] R. K. Pal, M. Schaeffer, and M. Ruzzene, J. Appl. Phys. **119**, 084305 (2016).
[13] L. Lu, Z. Wang, D. Ye, L. Ran, L. Fu, J. D. Joannopoulos, and M. Soljačić, Science **349**, 622 (2015).
[14] L. Lu, J. D. Joannopoulos, and M. Soljačić, Nat. Phys. **12**, 626 (2016).
[15] L. Lu, J. D. Joannopoulos, and M. Soljačić, Nat. Photonics **8**, 821 (2014).
[16] L. Lu, L. Fu, J. D. Joannopoulos, and M. Soljačić, Nat. Photonics **7**, 294 (2013).
[17] L. Wang, S.-K. Jian, and H. Yao, Phys. Rev. A **93**, 061801 (2016).
[18] B. Yang, Q. Gao, B. Tremain, R. Liu, L. E. Barr, Q. Yan, W. Gao, H. Liu, Y. Xiang, J. Chen, C. Fang, A. Hibbins, L. Lu, and S. Zhang, Science **359**, 1013 (2018).
[19] H. Ge, X. Ni, Y. Tian, S. K. Gupta, M.-H. Lu, X. Lin, W.-D. Huang, C. T. Chan, and Y.-F. Chen, Phys. Rev. Appl. **10**, 014017 (2018).
[20] H. He, C. Qiu, L. Ye, X. Cai, X. Fan, M. Ke, F. Zhang, and Z. Liu, Nature **560**, 61 (2018).
[21] T. Liu, S. Zheng, H. Dai, D. Yu, and B. Xia, arXiv:1803.04284.
[22] F. Li, X. Huang, J. Lu, J. Ma, and Z. Liu, Nat. Phys. **14**, 30 (2017).
[23] C. Fang, M. J. Gilbert, X. Dai, and B. A. Bernevig, Phys. Rev. Lett. **108**, 266802 (2012).
[24] X.-Y. Mai, D.-W. Zhang, Z. Li, and S.-L. Zhu, Phys. Rev. A **95**, 063616 (2017).
[25] B. Sbierski, M. Trescher, E. J. Bergholtz, and P. W. Brouwer, Phys. Rev. B **95**, 115104 (2017).
[26] L.-J. Lang, S.-L. Zhang, K. T. Law, and Q. Zhou, Phys. Rev. B **96**, 035145 (2017).
[27] Q. Chen and G. A. Fiete, Phys. Rev. B **93**, 155125 (2016).
[28] N. Xu, H. M. Weng, B. Q. Lv, C. E. Matt, J. Park, F. Bisti, V. N. Strocov, D. Gawryluk, E. Pomjakushina, K. Conder, N. C. Plumb, M. Radovic, G. Autes, O. V. Yazyev, Z. Fang, X. Dai, T. Qian, J. Mesot, H. Ding, and M. Shi, Nat. Commun. **7**, 11006 (2016).

Correction: The previously published Figure 4 contained wrong panels and has been replaced.